nanomaterials

MDPI

Article

Indefinite Graphene Nanocavities with Ultra-Compressed Mode Volumes

Chunchao Wen [1,2], Zongyang Wang [1,2], Jipeng Xu [1,2], Wei Xu [1,2], Wei Liu [1,2], Zhihong Zhu [1,2], Jianfa Zhang [1,2,*] and Shiqiao Qin [1,2]

[1] College of Advanced Interdisciplinary Studies, National University of Defense Technology, Changsha 410073, China; alexander_wen@yeah.net (C.W.); wzybiu@163.com (Z.W.); xjphn123@163.com (J.X.); weixu08a@163.com (W.X.); wei.liu.pku@gmail.com (W.L.); zzhwcx@163.com (Z.Z.); sqqin8@nudt.edu.cn (S.Q.)

[2] Hunan Provincial Key Laboratory of Novel Nano-Optoelectronic Information Materials and Devices, Changsha 410073, China

* Correspondence: jfzhang85@nudt.edu.cn

Abstract: Explorations of indefinite nanocavities have attracted surging interest in the past few years as such cavities enable light confinement to exceptionally small dimensions, relying on the hyperbolic dispersion of their consisting medium. Here, we propose and study indefinite graphene nanocavities, which support ultra-compressed mode volumes with confinement factors up to 10^9. Moreover, the nanocavities we propose manifest anomalous scaling laws of resonances and can be effectively excited from the far field. The indefinite graphene cavities, based on low dimensional materials, present a novel rout to squeeze light down to the nanoscale, rendering a more versatile platform for investigations into ultra-strong light–matter interactions at mid-infrared to terahertz spectral ranges.

Keywords: graphene indefinite cavities; anomalous scaling rules; hyperbolic medium metamaterial; mode volumes

Citation: Wen, C.; Wang, Z.; Xu, J.; Xu, W.; Liu, W.; Zhu, Z.; Zhang, J.; Qin, S. Indefinite Graphene Nanocavities with Ultra-Compressed Mode Volumes. *Nanomaterials* **2022**, *12*, 4004. https://doi.org/10.3390/nano12224004

Academic Editor: Giancarlo Rizza

Received: 26 September 2022
Accepted: 11 November 2022
Published: 14 November 2022

1. Introduction

Optical nanocavities provide a indispensable platform to study various sorts of light–matter interactions, including light emission [1–3], optical nonlinearity [4–6], optomechanics [7,8], and quantum effects [9,10]. Surface plasmonic modes can be employed to shrink optical cavities down to the subwavelength scale, and in particular, graphene plasmons have accessible simultaneous extraordinary confinement and flexible tenability, covering the spectral regimes from the the mid-infrared to terahertz (THz) ranges [11,12]. When a graphene sheet is placed close to a metal surface, it supports a special type of highly confined and low-loss electromagnetic mode called acoustic graphene plasmons [13,14], based on which an acoustic graphene plasmon nanocavity with ultra-compressed mode volumes can be achieved [15,16]. Resonant metastructures in the excitation of ultrasharp states with small mode volumes, such as toroidal resonances, surface lattice resonances, and bound states in the continuum, have also been mentioned in previous work. [17,18]

Recently, hyperbolic metamaterials (HMMs) and metasurfaces [19–23] have attracted much research interest. Hyperbolic media have different signs of the principal elements of the permittivity or permeability tensors, which can be exploited for applications concerning the enhancement of the optical density of states, heat-transfer engineering, nonlinear effects, optical forces, superlensing [24–30], optical topological transition [31–33], etc. [34]. The open and extended hyperbolic dispersion curves or surfaces [35] accommodate propagating waves with huge wave vectors that are essential for optical cavity miniaturization [36–38]. To be specific, hyperbolic dispersions have been achieved in nanowire arrays [39,40] and layered metal-dielectric structures [41,42], based on which

indefinite optical cavities have been obtained from the visible to near-infrared spectral regions. Besides metallic structures, HMMs based on 2D material such as graphene [43–45] in mid-infrared and terahertz ranges have also been proposed. Nevertheless, the possibilities of constructing indefinite nanocavities by relying on graphene-based HMMs and their contrasting optical properties have not been sufficiently explored.

In this article, we demonstrated a novel type of graphene indefinite nanocavity consisting of alternating graphene and silicon layers. The hyperbolic dispersion of such graphene-silicon HMM allows for propagating waves with large wave vectors and high effective indexes. This leads to ultra-confined modes with volume confinement factors up to 10^9. Moreover, such modes show anomalous scaling rules compared to conventional optical cavities. The indefinite graphene nanocavity can be efficiently excited by far-field illuminations over a broadband range, and its capability to confine light into tiny dimensions can play a significant role in infrared spectroscopy [46], biosensing [47,48], and other applications [49,50], over the spectral regime from mid-infrared to THz.

2. Theoretical Model

The scheme for an indefinite graphene nanocavity is presented in Figure 1a, which consists of layered graphene-silicon HMMs. Figure 1b represents the 2D cavity array. In both scenarios, the thickness of single-layer dielectric silicon is d = 9 nm and its relative permittivity is set to be ϵ_d = 11.56. The graphene can be effectively treated as a surface current sheet characterized by its surface electric conductivity σ: $\sigma = \sigma_{inter} + \sigma_{intra}$, where σ_{inter} and σ_{intra} denote contributions from the inter-band and intra-band transition of electrons, respectively [51]:

$$\sigma_{intra} = \frac{2ie^2 K_B T}{\pi\hbar^2(\omega + i/\tau)} \ln\left(2\cosh\left(\frac{E_F}{2K_B T}\right)\right) \quad (1)$$

$$\sigma_{inter} = \frac{e^2}{4}\left(\frac{1}{2} + \frac{1}{\pi}\arctan\frac{(\hbar\omega - 2E_F)}{2K_B T} - \frac{i}{2\pi}\ln\frac{(\hbar\omega + 2E_F)^2}{(\hbar\omega - 2E_F)^2 + (2K_B T)^2}\right) \quad (2)$$

where T is temperature; K_B is Boltzmann constant; e is elementary electric charge; and $\hbar$ is the reduced Planck constant. In this research, T = 300 K, $\tau = \mu E_F / eV_F^2$, $V_F = c/300$ is the Femi velocity, the carrier mobility of graphene $\mu = 10^4$ cm^2(vs)$^{-1}$, and the chemical potential of doping graphene E_F = 0.64 eV. Detailed simulation methods can be referred to Appendix A.

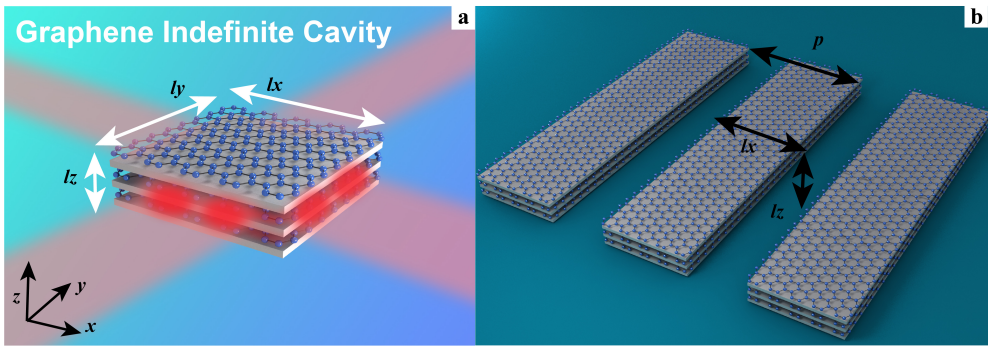

Figure 1. Schematic of the graphene indefinite nanocavity.(**a**). Perspective view of the a nanocavity made of mulilayered graphene-silicon HMM with indefinite permittivity. (**b**). 2D graphene indefinite cavity array.

3. Results And Disscussion

3.1. Dispersion and Resonance Conditions

The iso-frequency contour of HMM is calculated from the following relation [52] at f_0 = 30 THz for transverse-magnetic polarized mode, which belongs to type II HMM [35]:

$$\cos(k_z d) = \cosh(\gamma d) - \frac{\gamma\beta}{2}\sinh(\gamma d) \tag{3}$$

where $\beta = -Z_0\sigma i/\epsilon_d k_0$, $Z_0 = \sqrt{\mu_0/\epsilon_0}$ is the vacuum impedance and $\gamma = \sqrt{k_x^2 - \epsilon_d k_0^2}$. This HMM is effectively isotropic on the transverse x-y plane [53]: $\epsilon_x = \epsilon_y = \epsilon_d + i\sigma Z_0/k_0 d$ and $\epsilon_z = \epsilon_d$, indicating that the layered graphene-dielectric structure is effectively uniaxially anisotropic. The effective longitudinal permittivity along z (ϵ_z) equals the permittivity of silicon and remains positive, while the transverse effective permittivity can be negative due to the material dispersion of the monolayer graphene. A conventional optical cavity is limited by the closed iso-frequency contours of the consisting medium. However, much larger wave vectors are allowed in this HMM, which sustain ultra-compressed mode-volumes of the indefinite optical cavity.

Cavity modes in the graphene indefinite cavity and the iso-frequency contour of HMM are both shown in Figure 2. Here, the red stars represent the resonant wave vectors of the graphene indefinite cavity (see Figure 3A–F) calculated through the Fabry–Perot resonant condition:

$$\delta\phi_i + Re(k_i)l_i = m_i\pi, \quad i = x, y, z, \tag{4}$$

where the $\delta\phi_i$ is the boundary phase shift; k_i is the wave vector of mode; the integer m_i represents the mode order; and l_x, l_y, and l_z are the length of a single cavity along the x, y, and z-directions, respectively. We assume that l_y is infinite for 2D indefinite cavities (see Figure 1b) and $l_x = l_y$ for 3D indefinite cavities and confine our discussion to the special scenario of $k_x = k_y$.

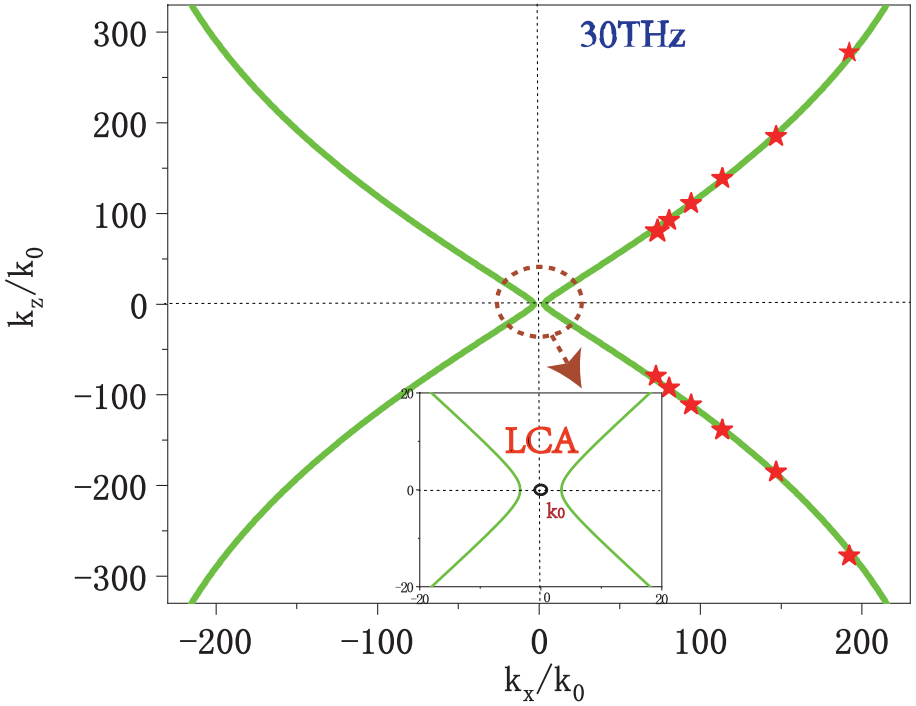

Figure 2. Iso-frequency contour of the graphene-silicon HMM in x-z plane at 30THz. Hyperbolic curves (green line) represent allowed propagating modes inside the multilayered metamaterial (calculated from Equation (3)), and the red stars denote resonant cavity modes. The black circle with radius k_0 around the origin represents a cross section of light cone in air (LCA).

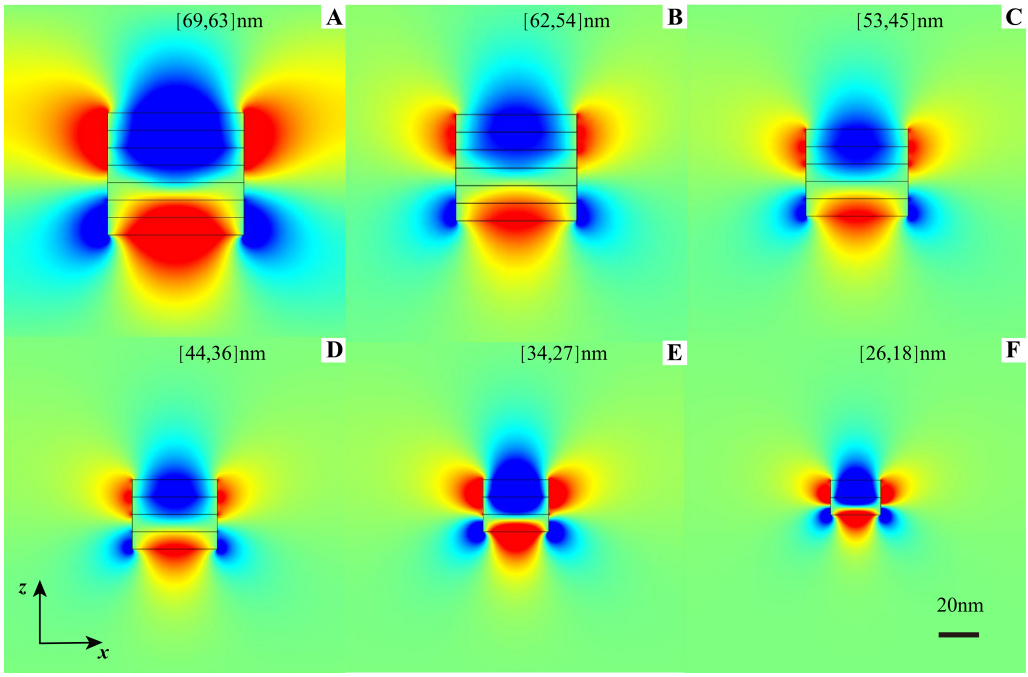

Figure 3. Mode distribution profiles with different cavity sizes. Electric field E_x of the (1, 1) mode for graphene indefinite nanoscale cavities with different (width, height) sizes but at the same resonant frequency 30THz.

3.2. Anomalous Scaling Rules of Graphene Indefinite Nanocavities

The spatial distributions of the electric field for a 2D indefinite cavity (see Figure 1b) are presented in Figure 3. It is clear that identical optical modes in these six cavities with different sizes (l_x, l_z) can be supported with the same resonant frequency and the same mode order (m_x, m_z) = (1, 1), and the confinement ability is comparable to that of acoustic graphene plasmon modes [15,54]. Indefinite graphene cavities with different sizes can resonate at a fixed frequency as long as the required resonant wave vectors are located on the the same iso-frequency contour. This means that the resonant wave vector can move along the iso-frequency curve as the size of the cavity scales down, which is not possible for conventional optical cavities. For example, the refractive indices (n_x, n_z) = (k_x/k_0, k_z/k_0) for a graphene indefinite cavity with the size combinations (62, 54), (44, 36), and (26, 18) nm are (80.6, 92.5), (113.6, 138.8), and (192.2, 277.6), respectively, all located on the iso-frequency curve. We can further shrink the dielectric thickness, making the effective mode index along z reach almost 300. However, the quantum effect should then be taken into consideration if the distance between neighbouring graphene sheets goes into the sub-nanometer regime.

Figure 4A–F shows the electric field distributions of the cavity modes with a fixed size [63, 54] nm for modes of different orders (2, m_z). In sharp contrast to conventional cavities, the higher-order mode resonates at lower frequencies, which are manifest in Figure 4. This is because the transverse and longitudinal components of the effective permittivity tensor (ϵ_x <0 and ϵ_z >0) of this bulk HMM have opposite signs. When the mode order m_z increases, the larger resonant k_z corresponds to a lower resonant frequency according to the following characteristic hyperbolic dispersion relation [44]:

$$k_x{}^2/\epsilon_z + k_z{}^2/\epsilon_x = \omega^2/c^2 \quad (5)$$

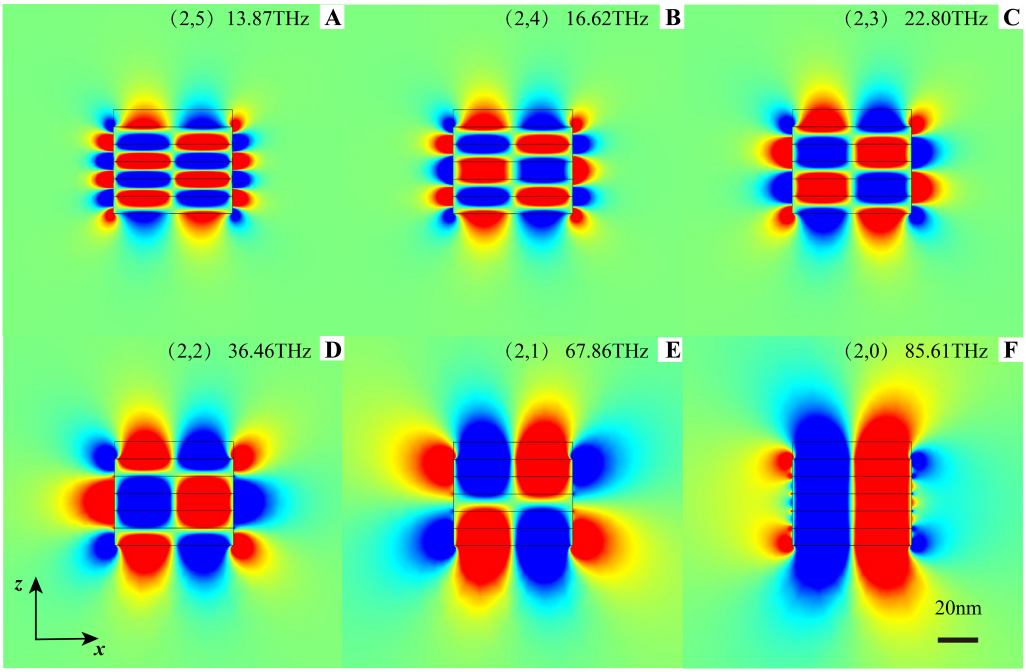

Figure 4. Resonate frequency with different mode order. Electric field E_x of six cavity modes (2, m_z) with different resonate frequencies but at the same cavity size [62, 54] nm.

3.3. Far-Field Excitation of Indefinite Graphene Nanocavities

As a next step, we perform simulations of a 2D nanocavity array (see Figure 1b) with 50% filling ratio for different cavity sizes (i.e., the period of cavity array $p = 2l_x$), which is illuminated by a far-field free-space plane wave. Figure 5 shows the transmission spectra for (1, 1) modes resonant at the same resonant frequency of 37THz for cavities of different sizes. As is also evident from Figure 5, for any cavity of a fixed size, the lower-order (1, 0) mode exhibits a higher resonant frequency than that of the higher-order (1, 1) mode, confirming the anomalous scaling rules discussed in the previous section.

3.4. Ultra-Compressed Mode Volumes of Graphene Indefinite Nanocavities

As a last step, we study the mode volume of graphene indefinite cavities by means of quasi-normal mode theory [15]. Figure 6 shows the obtained normalized mode volume of a 3D graphene indefinite cavity (red symbol and line), defined as V_{ca}/λ_0^3, where $V_{ca} = l_x l_y l_z$ (for the different vertical size l_z, we can calculate the vertical wave vector k_z by the z-direction Fabry—Perot resonant condition by Formula (4). In the next step, the tangential wave vector k_x and the tangential size l_x of the small cavity can be obtained by the hyperbolic iso-frequency contour shown in Figure 2 and the x-direction cavity resonant condition. Because the effective permittivity is isotropic and unchanged along all tangential directions for a multilayer system, we can assume the $k_y = k_x$ and $l_x = l_y$ for a 3D cavity roughly characterizes the mode volume. A bowtie photonic crystal cavity with a recorded deep subwavelength mode confinement factor 10^{-5}~10^{-4} [55] and similar metal-insulator-metal (MIM) indefinite cavities have beem experimentally demonstrated, and in the near-infrared range they have also been shown to obtain great field confinement [41]. Although the resonant wavelength of the graphene indefinite cavity (approximately 10 μm here, or longer wavelengths) is much larger than that of the MIM indefinite cavity (approximately 2 μm; refer to Ref. [41]), the obtained normalized mode volume of our graphene indefinite cavities can reach up to 10^{-9} (that is, a mode-volume confinement factor up to 10^{-9}), which is approximately two orders of magnitude smaller than that of the indefinite MIM cavities). The normalized mode volumes achieved here are comparable to the recently reported acoustic graphene plasmon cavities [15]. The extraordinary confinement we have achieved

mainly relies on the open hyperbolic dispersion curves, which can be employed to further squeeze light down to atomic scales [54].

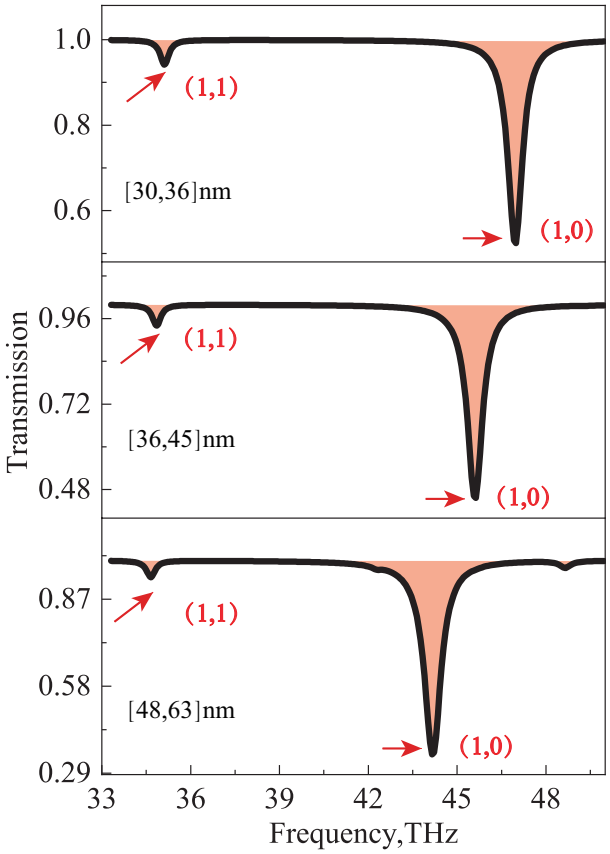

Figure 5. Transmission spectra of periodic indefinite nanoscale cavity array. 1D cavity array with a 50% cavity area filling ratio for different cavity sizes. Both higher−order (1, 1) and lower−order (1, 0) modes are indicated. All (1, 1) modes resonate at the same frequency of 37 THz, and lower order (1, 0) modes resonate at other higher higher frequencies.

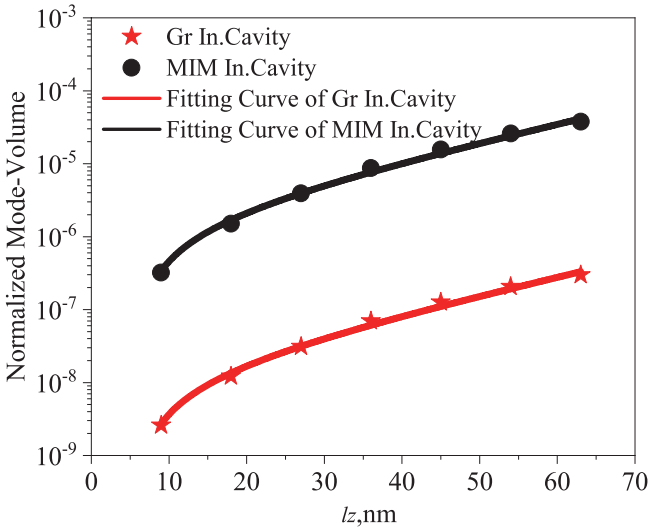

Figure 6. The obtained normalized mode−volume of indefinite cavities. Graphene indefinite cavities resonate at the far−infrared spectrum, where red symbols are calculated from the cavities in Figure 3, the red line is the fitting curve and MIM indefinite cavity resonates at the near−infrared range (black), calculated from reference [41], as function of the different length l_z of a single indefinite nanoscale cavity.

4. Conclusions

In conclusion, we propose and demonstrate graphene indefinite nanocavities with ultra-compressed mode volumes and extraordinary optical confinement at mid-infrared and THz spectral regimes. The normalized mode volume can reach approximately 10^{-9}, two orders of magnitude smaller than the widely studies MIM indefinite cavities. Our indefinite graphene nanocavities can be efficiently excited from the far field and manifest anomalous scaling laws of the resonances, which can function as a promising playground to study extreme light–matter interactions and explore tunable high-performance metadevices with desired functionalities.

Author Contributions: Conceptualization, J.Z. and C.W.; methodology, C.W.; software, C.W.; validation, Z.W. and Z.Z.; formal analysis, J.X.; investigation, W.X.; resources, J.Z.; data curation, W.L.; writing—original draft preparation, C.W.; writing—review and editing, W.L.; visualization, C.W.; supervision, Z.Z.; project administration, S.Q.; and funding acquisition, J.Z. All authors have read and agreed to the published version of the manuscript.

Funding: This research was funded by the Science and Technology Planning Project of Hunan Province (2018JJ1033 and 2017RS3039), the National Natural Science Foundation of China (11304389 and 11674396), and the National University of Defense Technology (ZK18-03-05).

Data Availability Statement: Relevant data is included in the manuscript.

Conflicts of Interest: The authors declare no conflict of interest.

Appendix A

Numerical Simulations: The proposed system is calculated with numerical simulations (commercially available finite element software COMSOL multiphysics). A surface current density boundary condition $J = \sigma E$ in software is employed to describe the electric properties of graphene. In order to explore the spatial distributions of the electric field for a 2D indefinite cavity with a different cavity size at a chosen resonating frequency, the mode analysis section in the model builder window and the study node of COMSOL Multiphysics are used. Before numerical simulation, the tangential and vertical dimensions of the small cavity can roughly be estimated by the iso-frequency contour of the HMMs and the Fabry–-Perot resonant condition. (l_x, l_z) of the cavity size are set in the simulation model, respectively. Meanwhile, for the Eigenfrequency section in the model-builder window, the study node of COMSOL Multiphysics is used to calculate the resonate frequency with a different mode order but at the same cavity size. As for the spectra response, the simulation nanocavity array with a far-field free-space plane wave at normal incidence by Port excitation in COMSOL software is performed. The electric field direction of the incident wave is along the x-direction. The periodic boundary conditions are applied along the x-direction, and the perfect matched layer conditions are applied along the z-direction.

References

1. Adamo, G.; MacDonald, K.F.; Fu, Y.; Wang, C.; Tsai, D.; De Abajo, F.G.; Zheludev, N. Light well: A tunable free-electron light source on a chip. *Phys. Rev. Lett.* **2009**, *103*, 113901. [CrossRef] [PubMed]
2. Khajavikhan, M.; Simic, A.; Katz, M.; Lee, J.; Slutsky, B.; Mizrahi, A.; Lomakin, V.; Fainman, Y. Thresholdless nanoscale coaxial lasers. *Nature* **2012**, *482*, 204–207. [CrossRef] [PubMed]
3. Kotal, S.; Artioli, A.; Wang, Y.; Osterkryger, A.D.; Finazzer, M.; Fons, R.; Genuist, Y.; Bleuse, J.; Gérard, J.M.; Gregersen, N.; et al. A nanowire optical nanocavity for broadband enhancement of spontaneous emission. *Appl. Phys. Lett.* **2021**, *118*, 194002. [CrossRef]
4. Zhang, L.; Wu, F.; Hou, S.; Zhang, Z.; Chou, Y.H.; Watanabe, K.; Taniguchi, T.; Forrest, S.R.; Deng, H. Van der Waals heterostructure polaritons with moire-induced nonlinearity. *Nature* **2021**, *591*, 61. [CrossRef] [PubMed]
5. Xingqiao, C.; Jianfa, Z.; Chunchao, W.; Ken, L.; Zhihong, Z.; Shiqiao, Q.; Xiaodong, Y. Optical nonlinearity and non-reciprocal transmission of graphene integrated metasurface. *Carbon* **2021**, *173*, 126–134. [CrossRef]
6. Shi, J.; Guo, Q.; Shi, Z.; Zhang, S.; Xu, H. Nonlinear nanophotonics based on surface plasmon polaritons. *Appl. Phys. Lett.* **2021**, *119*, 130501. [CrossRef]

7. Chen, W.; Roelli, P.; Hu, H.; Verlekar, S.; Amirtharaj, S.P.; Barreda, I, A.; Kippenberg, T.J.; Kovylina, M.; Verhagen, E.; Martinez, A.; et al. Continuous-wave frequency upconversion with a molecular optomechanical nanocavity. *Science* **2021**, *374*, 1264. [CrossRef]
8. Favero, I.; Karrai, K. Optomechanics of deformable optical cavities. *Nat. Photonics* **2009**, *3*, 201–205. [CrossRef]
9. Xie, X.; Zhang, W.; He, X.; Wu, S.; Dang, J.; Peng, K.; Song, F.; Yang, L.; Ni, H.; Niu, Z.; et al. Cavity Quantum Electrodynamics with Second-Order Topological Corner State. *Laser Photon. Rev.* **2020**, *14*, 1900425. [CrossRef]
10. He, Z.; Han, Z.; Yuan, J.; Sinyukov, A.M.; Eleuch, H.; Niu, C.; Zhang, Z.; Lou, J.; Hu, J.; Voronine, D.V.; et al. Quantum plasmonic control of trions in a picocavity with monolayer WS2. *Sci. Adv.* **2019**, *5*, 8763. [CrossRef]
11. Li, X.; Tao, L.; Chen, Z.; Fang, H.; Li, X.; Wang, X.; Xu, J.B.; Zhu, H. Graphene and related two-dimensional materials: Structure-property relationships for electronics and optoelectronics. *Appl. Phys. Rev.* **2017**, *4*, 021306. [CrossRef]
12. Gan, X.; Englund, D.; Van Thourhout, D.; Zhao, J. 2D materials-enabled optical modulators: From visible to terahertz spectral range. *Appl. Phys. Rev.* **2022**, *9*, 021302. [CrossRef]
13. Alonso-Gonzalez, P.; Nikitin, A.Y.; Gao, Y.; Woessner, A.; Lundeberg, M.B.; Principi, A.; Forcellini, N.; Yan, W.; Velez, S.; Huber, A.J.; et al. Acoustic terahertz graphene plasmons revealed by photocurrent nanoscopy. *Nat. Nanotechnol.* **2017**, *12*, 31–35. [CrossRef] [PubMed]
14. Lee, I.H.; Yoo, D.; Avouris, P.; Low, T.; Oh, S.H. Graphene acoustic plasmon resonator for ultrasensitive infrared spectroscopy. *Nat. Nanotechnol.* **2019**, *14*, 313. [CrossRef]
15. Epstein, I.; Alcaraz, D.; Huang, Z.; Pusapati, V.V.; Hugonin, J.P.; Kumar, A.; Deputy, X.M.; Khodkov, T.; Rappoport, T.G.; Hong, J.Y.; et al. Far-field excitation of single graphene plasmon cavities with ultracompressed mode volumes. *Science* **2020**, *368*, 1219. [CrossRef]
16. Wen, C.; Chen, X.; Zhang, J.; Xu, W.; Luo, J.; Zhou, Y.; Zhu, Z.; Qin, S.; Yuan, X. Far-Field Excitation of Acoustic Graphene Plasmons with a Metamaterial Absorber. *Adv. Photonics Res.* **2021**, *2*, 2000066. [CrossRef]
17. Wang, B.; Yu, P.; Wang, W.; Zhang, X.; Kuo, H.C.; Xu, H.; Wang, Z.M. High-Q Plasmonic Resonances: Fundamentals and Applications. *Adv. Opt. Mater.* **2021**, *9*, 2001520. [CrossRef]
18. Ahmadivand, A.; Gerislioglu, B.; Ahuja, R.; Mishra, Y.K. Toroidal Metaphotonics and Metadevices. *Laser Photon. Rev.* **2020**, *14*, 1900326. [CrossRef]
19. Poddubny, A.; Iorsh, I.; Belov, P.; Kivshar, Y. Hyperbolic metamaterials. *Nat. Photonics* **2013**, *7*, 948–957. [CrossRef]
20. Li, P.; Dolado, I.; Javier Alfaro-Mozaz, F.; Casanova, F.; Hueso, L.E.; Liu, S.; Edgar, J.H.; Nikitin, A.Y.; Velez, S.; Hillenbrand, R. Infrared hyperbolic metasurface based on nanostructured van der Waals materials. *Science* **2018**, *359*, 892. [CrossRef]
21. Aigner, A.; Dawes, J.M.; Maier, S.A.; Ren, H. Nanophotonics shines light on hyperbolic metamaterials. *Light Sci. Appl.* **2022**, *11*, 26. [CrossRef] [PubMed]
22. Gomez-Diaz, J.S.; Alu, A. Flatland Optics with Hyperbolic Metasurfaces. *ACS Photonics* **2016**, *3*, 2211–2224. [CrossRef]
23. Sun, J.; Litchinitser, N.M.; Zhou, J. Indefinite by Nature: From Ultraviolet to Terahertz. *ACS Photonics* **2014**, *1*, 293–303. [CrossRef]
24. Ferrari, L.; Smalley, J.S.T.; Fainman, Y.; Liu, Z. Hyperbolic metamaterials for dispersion-assisted directional light emission. *Nanoscale* **2017**, *9*, 9034–9048. [CrossRef] [PubMed]
25. Kitur, J.K.; Gu, L.; Tumkur, T.; Bonner, C.; Noginov, M.A. Stimulated Emission of Surface Plasmons on Top of Metamaterials with Hyperbolic Dispersion. *ACS Photonics* **2015**, *2*, 1019–1024. [CrossRef]
26. Wu, X.; McEleney, C.A.; Gonzalez-Jimenez, M.; Macedo, R. Emergent asymmetries and enhancement in the absorption of natural hyperbolic crystals. *Optica* **2019**, *6*, 1478–1483. [CrossRef]
27. Li, J.; Hu, G.; Shi, L.; He, N.; Li, D.; Shang, Q.; Zhang, Q.; Fu, H.; Zhou, L.; Xiong, W.; et al. Full-color enhanced second harmonic generation using rainbow trapping in ultrathin hyperbolic metamaterials. *Nat. Commun.* **2021**, *12*, 6425. [CrossRef]
28. Jin, R.; Xu, Y.; Dong, Z.G.; Liu, Y. Optical Pulling Forces Enabled by Hyperbolic Metamaterials. *Nano Lett.* **2021**, *21*, 10431–10437. [CrossRef]
29. Gelkop, Y.; Di Mei, F.; Frishman, S.; Garcia, Y.; Falsi, L.; Perepelitsa, G.; Conti, C.; DelRe, E.; Agranat, A.J. Hyperbolic optics and superlensing in room-temperature KTN from self-induced k-space topological transitions. *Nat. Commun.* **2021**, *12*, 7241. [CrossRef]
30. Liu, L.; Gao, P.; Liu, K.; Kong, W.; Zhao, Z.; Pu, M.; Wang, C.; Luo, X. Nanofocusing of circularly polarized Bessel-type plasmon polaritons with hyperbolic metamaterials. *Mater. Horiz.* **2017**, *4*, 290–296. [CrossRef]
31. Hu, G.; Krasnok, A.; Mazor, Y.; Qu, C.W.; Alu, A. Moire Hyperbolic Metasurfaces. *Nano Lett.* **2020**, *20*, 3217–3224. [CrossRef] [PubMed]
32. Yali, Z.; Qingdong, O.; Lu, L.; Chunqi, Z.; Ziyu, W.; Youning, G.; Xiang, L.; Yupeng, Z.; Guangwei, H.; Zhilin, Y.; et al. Tailoring Topological Transitions of Anisotropic Polaritons by Interface Engineering in Biaxial Crystals. *Nano Lett.* **2022**, *20*, 4260–4268. [CrossRef]
33. Chen, J.; Lin, X.; Chen, M.; Low, T.; Chen, H.; Dai, S. A perspective of twisted photonic structures. *Appl. Phys. Lett.* **2021**, *119*, 240501. [CrossRef]
34. Passler, N.C.; Ni, X.H.; Hu, G.; Matson, J.R.; Garini, G.; Wolf, M.; Schubert, M.; Alu, A.; Caldwell, J.D.; Folland, T.G.; et al. Hyperbolic shear polaritons in low-symmetry crystals. *Nature* **2021**, *602*, 595–600. [CrossRef]
35. Dasol, L.; Sunae, S.; Guangwei, H.; Minkyung, K.; Trevon, B.; Hanlyun, C.; Jaekyung, K.; Hongyoon, K.; ChengWei, Q.; Junsuk, R. Hyperbolic metamaterials: Fusing artificial structures to natural 2D materials. *eLight* **2022**, *2*, 01–23. [CrossRef]

36. Indukuri, S.R.K.C.; Bar-David, J.; Mazurski, N.; Levy, U. Ultrasmall Mode Volume Hyperbolic Nanocavities for Enhanced Light-Matter Interaction at the Nanoscale. *ACS Nano* **2019**, *13*, 11770–11780. [CrossRef]
37. Zhu, B.; Ren, G.; Zheng, S.; Lin, Z.; Jian, S. Nanoscale dielectric-graphene-dielectric tunable infrared waveguide with ultrahigh refractive indices. *Opt. Express* **2013**, *21*, 17089–17096. [CrossRef]
38. Wang, Q.; Hou, L.; Li, C.; Zhou, H.; Gan, X.; Liu, K.; Xiao, F.; Zhao, J. Toward high-performance refractive index sensor using single Au nanoplate-on-mirror nanocavity. *Nanoscale* **2022**, *14*, 10773–10779. [CrossRef]
39. Yao, J.; Yang, X.; Yin, X.; Bartal, G.; Zhang, X. Three-dimensional nanometer-scale optical cavities of indefinite medium. *Proc. Acad. Natl. Sci. USA* **2011**, *108*, 11327–11331. [CrossRef]
40. Bisht, A.; He, W.; Wang, X.; Wu, L.Y.L.; Chen, X.; Li, S. Hyperlensing at NIR frequencies using a hemispherical metallic nanowire lens in a sea-urchin geometry. *Nanoscale* **2016**, *8*, 10669–10676. [CrossRef]
41. Yang, X.; Yao, J.; Rho, J.; Yin, X.; Zhang, X. Experimental realization of three-dimensional indefinite cavities at the nanoscale with anomalous scaling laws. *Nat. Photonics* **2012**, *6*, 450–454. [CrossRef]
42. Yan, R.; Wang, T.; Wang, H.; Yue, X.; Wang, L.; Wang, Y.; Zhang, J. Effective excitation of bulk plasmon-polaritons in hyperbolic metamaterials for high-sensitivity refractive index sensing. *J. Mater. Chem. C* **2022**, *10*, 5200–5209. [CrossRef]
43. Iorsh, I.V.; Mukhin, I.S.; Shadrivov, I.V.; Belov, P.A.; Kivshar, Y.S. Hyperbolic metamaterials based on multilayer graphene structures. *Phys. Rev. B* **2013**, *87*, 075416. [CrossRef]
44. Chang, Y.C.; Liu, C.H.; Liu, C.H.; Zhang, S.; Marder, S.R.; Narimanov, E.E.; Zhong, Z.; Norris, T.B. Realization of mid-infrared graphene hyperbolic metamaterials. *Nat. Commun.* **2016**, *7*, 10568. [CrossRef]
45. Dudek, M.; Kowerdziej, R.; Pianelli, A.; Parka, J. Graphene-based tunable hyperbolic microcavity. *Sci. Rep.* **2021**, *11*, 74. [CrossRef]
46. Nong, J.; Tang, L.; Lan, G.; Luo, P.; Li, Z.; Huang, D.; Yi, J.; Shi, H.; Wei, W. Enhanced Graphene Plasmonic Mode Energy for Highly Sensitive Molecular Fingerprint Retrieval. *Laser Photon. Rev.* **2021**, *15*, 2000300. [CrossRef]
47. Xu, L.; Zhang, X.; Wang, Z.; Haidry, A.A.; Yao, Z.; Haque, E.; Wang, Y.; Li, G.; Daeneke, T.; McConville, C.F.; et al. Low dimensional materials for glucose sensing. *Nanoscale* **2021**, *13*, 11017–11040. [CrossRef] [PubMed]
48. Cheng, Y.; Ren, B.; Xu, K.; Jeerapan, I.; Chen, H.; Li, Z.; Ou, J.Z. Recent progress in intrinsic and stimulated room-temperature gas sensors enabled by low-dimensional materials. *J. Mater. Chem. C* **2021**, *9*, 3026–3051. [CrossRef]
49. Wen, C.; Luo, J.; Xu, W.; Zhu, Z.; Qin, S.; Zhang, J. Enhanced Molecular Infrared Spectroscopy Employing Bilayer Graphene Acoustic Plasmon Resonator. *Biosensors* **2021**, *11*, 431. [CrossRef]
50. Gowda, P.; Patient, D.A.; Horsley, S.A.R.; Nash, G.R. Toward efficient and tailorable mid-infrared emitters utilizing multilayer graphene. *Appl. Phys. Lett.* **2022**, *120*, 051105. [CrossRef]
51. Falkovsky, L.A. Optical properties of graphene. In *Journal of Physics: Conference Series*; IOP Publishing: Bristol, UK, 2008; Volume 129, p. 012004. [CrossRef]
52. Wang, B.; Zhang, X.; Garcia-Vidal, F.J.; Yuan, X.; Teng, J. Strong Coupling of Surface Plasmon Polaritons in Monolayer Graphene Sheet Arrays. *Phys. Rev. Lett.* **2012**, *109*, 073901. [CrossRef] [PubMed]
53. Sukham, J.; Takayama, O.; Mahmoodi, M.; Sychev, S.; Bogdanov, A.; Tavassoli, S.H.; Lavrinenko, A.V.; Malureanu, R. Investigation of effective media applicability for ultrathin multilayer structures. *Nanoscale* **2019**, *11*, 12582–12588. [CrossRef] [PubMed]
54. Alcaraz Iranzo, D.; Nanot, S.; Dias, E.J.C.; Epstein, I.; Peng, C.; Efetov, D.K.; Lundeberg, M.B.; Parret, R.; Osmond, J.; Hong, J.Y.; et al. Probing the ultimate plasmon confinement limits with a van der Waals heterostructure. *Science* **2018**, *360*, 291–295. [CrossRef] [PubMed]
55. Shuren, H.; Marwan, K.; Rafael, S.M.; Ernst, K.; Sebastian, E.; William, M.J.G.; Sharon, M.W. Experimental realization of deep-subwavelength confinement in dielectric optical resonators. *Sci. Adv.* **2018**, *4*, eaat2355. [CrossRef]